CrossMark

J. Fluid Mech. (2016), *vol.* 799, R1, doi:10.1017/jfm.2016.400

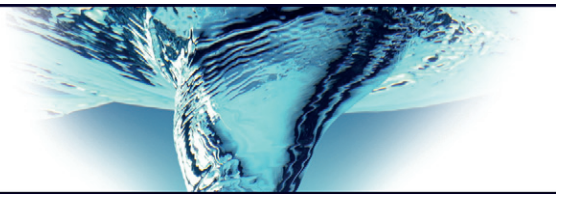

JFM RAPIDS
journals.cambridge.org/rapids

Turbulent Taylor–Couette flow with stationary inner cylinder

R. Ostilla-Mónico[1,2,†], R. Verzicco[1,3] and D. Lohse[1,4]

[1]Physics of Fluids Group, Mesa+ Institute and J.M. Burgers Centre for Fluid Dynamics, University of Twente, P.O. Box 217, 7500 AE Enschede, The Netherlands

[2]School of Engineering and Applied Sciences and Kavli Institute for Bionano Science and Technology, Harvard University, Cambridge, MA 02138, USA

[3]Dipartimento di Ingegneria Industriale, University of Rome 'Tor Vergata', Via del Politecnico 1, Roma 00133, Italy

[4]Max Planck Institute for Dynamics and Self-Organization, 37077 Göttingen, Germany

(Received 3 April 2016; revised 5 June 2016; accepted 8 June 2016;
first published online 21 June 2016)

A series of direct numerical simulations were performed of Taylor–Couette (TC) flow, the flow between two coaxial cylinders, with the outer cylinder rotating and the inner one fixed. Three cases were considered, where the Reynolds number of the outer cylinder was $Re_o = 5.5 \times 10^4$, $Re_o = 1.1 \times 10^5$ and $Re_o = 2.2 \times 10^5$. The ratio of radii $\eta = r_i/r_o$ was fixed to $\eta = 0.909$ to mitigate the effects of curvature. Axially periodic boundary conditions were used, with the aspect ratio of vertical periodicity Γ fixed to $\Gamma = 2.09$. Being linearly stable, TC flow with outer cylinder rotation is known to have very different behaviour than TC flow with pure inner cylinder rotation. Here, we find that the flow nonetheless becomes turbulent, but the torque required to drive the cylinders and level of velocity fluctuations was found to be smaller than those for pure inner cylinder rotation at comparable Reynolds numbers. The mean angular momentum profiles showed a large gradient in the bulk, instead of the constant angular momentum profiles of pure inner cylinder rotation. The near-wall mean and fluctuation velocity profiles were found to coincide only very close to the wall, showing large deviations from both pure inner cylinder rotation profiles and the classic von Karman law of the wall elsewhere. Finally, transport of angular velocity was found to occur mainly through intermittent bursts, and not through wall-attached large-scale structures as is the case for pure inner cylinder rotation.

Key words: Taylor–Couette flow, turbulence simulation, turbulent convection

† Email address for correspondence: rostillamonico@g.harvard.edu

© Cambridge University Press 2016

https://doi.org/10.1017/jfm.2016.400 Published online by Cambridge University Press

1. Introduction

Taylor–Couette (TC) flow, the flow between two coaxial and independently rotating cylinders, can present different types of transition to turbulence. For vanishing viscosity, TC flow is linearly unstable if $|r_o\omega_o| < |r_i\omega_i|$, where $r_{i,o}$ are the radii of the inner and outer cylinders, and $\omega_{i,o}$ their angular velocities (Rayleigh 1917), due to the centrifugal forces. If viscosity is considered, a minimum rotation strength is required to overcome the viscous damping. For pure inner cylinder rotation, once this stability threshold is crossed, TC flow presents a supercritical transition to turbulence, where the purely azimuthal flow develops large-scale structures that fill up the entire gap and effectively redistribute angular momentum (Taylor 1923; Fardin, Perge & Taberlet 2014). With increasing rotation, these large-scale structures undergo a series of transitions from laminar Taylor vortices to wavy Taylor vortices to modulated wavy Taylor vortices to turbulent Taylor vortices (Andereck, Liu & Swinney 1986). Even at very large Reynolds numbers these structures have been observed to persist in some regions of the parameter space, i.e. at $Re \sim O(10^5)$ in simulations (Ostilla-Monico *et al.* 2014*a*) and then at $Re \sim O(10^6)$ in experiments (Huisman *et al.* 2014). The flow field shows a clear lack of statistical spatial homogeneity and these 'rolls' cause substantially large deviations of the near-wall velocity profiles of TC flow from the classic wall-turbulence profiles of channels and pipes. This effect has been attributed to the role of curvature and the centrifugal instability (Ostilla-Mónico *et al.* 2016). For an overview of supercritical TC flow at large Reynolds numbers, we refer the reader to the review of Grossmann, Lohse & Sun (2016).

If, instead, the outer cylinder is rotated, and the inner cylinder is kept fixed, the flow undergoes a subcritical transition to turbulence. This transition is quite different from the supercritical transition detailed previously, as the flow does not go undergo a series of changes from less complex to more complex flow patterns, but instead makes a sudden transition to turbulence, either in localized spots or filling the entire gap. While Taylor (1936) found evidence for this subcritical transition by measuring the torques and how they deviated from the predictions for steady flow, this transition was first systematically studied by Coles (1965), who found that for low outer cylinder Reynolds numbers, $Re_o = dr_o\omega_o/\nu$ with ν the fluid kinematic viscosity and d the gap width, $d = r_o - r_i$, intermittent turbulent patches coexisted with laminar flow, with well-defined interfaces. The persistence time of these patches increased with increasing inner cylinder Reynolds number $Re_i = d\omega_i r_i/\nu$, and so did the turbulent fraction, until the flow was fully turbulent. For the lower Re_o range, the flow had to be started in a supercritical state, such that the centrifugal instabilities provided an initial perturbation for the generation of turbulence. For larger values of Re_o, the flow no longer required the centrifugal instability to transition to turbulence, and could remain exclusively in the subcritical region and still see a spontaneous, or 'catastrophic', transition to turbulence.

Studies of subcritical TC flow continued through the years, both theoretically, in an attempt to develop nonlinear stability criteria, as well as numerically and experimentally. The focus of many of these studies was on the sharp turbulent–laminar interface and on spiral turbulence, a particular flow where the bursts took a spiral shape (van Atta 1966; Andereck, Dickman & Swinney 1983). We refer the reader to the thesis of Borrero-Echeverry (2014) for a detailed historical overview of studies of subcritical TC flow. Subcritical transitions to turbulence have been well studied in the past, and are an active area of research, because not only TC flow, but also pipe and channel flows present a subcritical transition to turbulence. For a comprehensive overview of this field, we refer the reader to the review by Eckhardt *et al.* (2008).

https://doi.org/10.1017/jfm.2016.400 Published online by Cambridge University Press

A recent systematic study of pure outer cylinder rotation (OCR) in TC flow was performed by Burin & Czarnocki (2012), who experimentally studied in detail the effect of gap width and end-plate configurations on the transition to turbulence. These authors also performed velocimetry in the bulk and found that regions of high turbulence were associated with high shear. Earlier, Borrero-Echeverry, Schatz & Tagg (2010) had already provided evidence for superexponential dependence on the Reynolds number of the decay times of turbulence. Therefore, it seems that outer cylinder TC flow with high Reynolds number is turbulent for extremely long time scales. This regime has not been well characterized: Burin & Czarnocki (2012) did not provide velocimetry close to the walls. The other experimental studies by Paoletti & Lathrop (2011) and Paoletti *et al.* (2012) only provided torque measurements for pure OCR, which indicated values well above the values for laminar flow but also much lower than the torque values for pure inner cylinder rotation. However, experiments are limited by the necessary presence of end plates to provide flow confinement, and this could potentially affect the physics. Numerical studies of pure OCR in an infinite (periodic) domain are limited to Deguchi, Meseguer & Mellibovsky (2014), who considered Reynolds numbers near the transition to turbulence.

In this article, we conducted a series of direct numerical simulations (DNS) of axially periodic and fully turbulent TC flow with only outer cylinder rotation, in an attempt to isolate and study subcritical behaviour of TC flow, and to eliminate the effect of perturbations arising at the end plates. We consider pure outer cylinder rotation because it does not have the complex combination of sub- and supercritical behaviour seen in turbulent counter-rotating TC flow (van Gils *et al.* 2012; Brauckmann & Eckhardt 2013; Grossmann *et al.* 2016). The simulated TC geometry is a narrow-gap system, which produces very strong rolls in the case of pure inner cylinder rotation (ICR), and limits the effect of strong curvature, which causes very different flow physics (Ostilla-Mónico *et al.* 2016). In this article, we extend the analysis of Ostilla-Mónico *et al.* (2016) in an attempt to understand which pieces of the flow physics come from the centrifugal (in)stability and to reveal and quantify the differences between supercritical and subcritical TC turbulence.

2. Simulation details

The DNS were performed using an energy-conserving second-order centred finite-difference code with fractional time stepping (Verzicco & Orlandi 1996; van der Poel *et al.* 2015). This code has been extensively used and validated for TC flow. The ratio of radii $\eta = r_i/r_o$ was chosen as $\eta = 0.909$ as in Ostilla-Mónico *et al.* (2016), to mitigate curvature effects. The aspect ratio $\Gamma = L_z/d$, where L_z is the axial periodicity length, was taken as $\Gamma = 2.09$. To reduce computational costs, a rotational symmetry order $n_s = 20$ was imposed, which results in a minimum azimuthal extent of π-gap widths at the inner cylinder. This choice of n_{sym} and Γ results in computational boxes that are large enough to show sign changes of the azimuthal velocity autocorrelation functions at the mid-gap, as was already observed in Ostilla-Mónico, Verzicco & Lohse (2015) for pure inner cylinder rotation. The size of the time steps was chosen dynamically by imposing that the maximum Courant–Friedrichs–Lewy (CFL) number in the grid is 0.5.

Three different outer cylinder Reynolds numbers were simulated: $Re_o = 5.5 \times 10^4$, $Re_o = 1.1 \times 10^5$ and $Re_o = 2.2 \times 10^5$. These outer cylinder Reynolds numbers have an equivalent shear Reynolds number $Re_s = 2|\eta Re_o - Re_i|/(1+\eta)$ (Dubrulle *et al.* 2005) to pure ICR rotations at $Re_i = 5 \times 10^4$, $Re_i = 1 \times 10^5$ and $Re_i = 2 \times 10^5$. These Reynolds

https://doi.org/10.1017/jfm.2016.400 Published online by Cambridge University Press

numbers are much larger than the transitional Reynolds numbers for spiral turbulence $Re_o \sim 5000$ (Coles 1965; Andereck *et al.* 1983; Deguchi *et al.* 2014), and are in the regime where no spiral structures are seen in experiments (Burin & Czarnocki 2012). With the largest Reynolds number, an inner cylinder frictional Reynolds number $Re_{\tau,i} = u_{\tau,i}d/\nu$ of up to 1220 is achieved, where the frictional velocity of the inner cylinder is defined as $u_{\tau,i} = \sqrt{\tau_w/\rho}$ with τ_w the shear stress at the cylinder wall and ρ the fluid density. The outer cylinder frictional Reynolds number (velocity) is simply $Re_{\tau,o} = \eta Re_{\tau,i}$ ($u_{\tau,o} = \eta u_{\tau,i}$). For convenience we define the inner cylinder viscous length as $\delta_{\nu,i} = \nu/u_{\tau,i}$, the non-dimensional distance from the wall $\tilde{r} = (r - r_i)/d$, the non-dimensional axial coordinate $\tilde{z} = z/d$ and the non-dimensional angular velocity $\tilde{\omega} = \omega/\omega_o$, with the angular velocity $\omega = u_\theta/r$.

We also note that the lowest Reynolds number simulated is about one order of magnitude larger than the estimated Reynolds number for transition at $\eta = 0.909$ by Burin & Czarnocki (2012). It was impossible with our simulations to achieve stable turbulent states at Reynolds numbers lower than $Re_o = 5.5 \times 10^4$, probably due to the small computational box used. To perform the simulations, we first started a simulation with $Re_o = 1.1 \times 10^5$ and a stationary inner cylinder with white noise of $O(r_o\omega_o)$. After a very long transient of about 1000 large eddy turnover times based on $d/(r_o\omega_o\eta)$, a statistically stationary state was reached. The transients were significantly longer than those of pure ICR TC flow, because u_τ is a factor of two to three times smaller. This state was used as the initial condition for both the $Re_o = 2.2 \times 10^5$ and $Re_o = 5.5 \times 10^4$ simulations, and the mesh was either coarsened or refined to ensure a correct balance between accuracy and speed of computation. Attempting to start simulations at lower Re_o from initial conditions at $Re_o = 5.5 \times 10^4$ resulted in divergence of the fields for unclear reasons. If white noise of order $O(r_o\omega_o)$ was used at $Re_o = 1.1 \times 10^4$, the system would slowly relaminarize and return to the purely azimuthal, steady state.

After the transients, the simulations were run for (at least) an additional 67 large eddy turnover times based on $\tilde{t} = \eta r_o\omega_o t/d$. The temporal convergence was assured by checking the radial dependence of the angular velocity current J^ω, defined as $J^\omega = r^3(\langle u_r\omega\rangle_{\theta,z,t} - \nu\partial_r\langle\omega\rangle_{\theta,z,t})$ (Eckhardt, Grossmann & Lohse 2007), where $\langle\cdots\rangle_{x_i}$ denotes averaging with respect to x_i. J^ω should have no radial dependence when averaged for an infinite time; however, for finite-time statistics we considered that deviations smaller than 3 % from the average value in the bulk were sufficient, as these were associated with deviations of the time-averaged torque (J^ω at the cylinders) at both cylinders smaller than 1 %, a value we have used previously (Ostilla-Mónico *et al.* 2016). The computational domain was uniformly discretized in the azimuthal and axial directions, while a clipped Chebyshev-type clustering was used in the radial direction. Full details of the numerical resolution used are provided in table 1. The table includes pure ICR data (i.e. the I1 and I2 cases) from Ostilla-Mónico *et al.* (2016) (referred to there as R1 and R2) for comparison. The I1 case has the same Re_τ as the O2 case, while the I2 case has the same driving shear as the O2 case.

3. Results

We first focus on the torque to drive the cylinders. At comparable Reynolds numbers, a smaller torque is required for pure OCR than for pure ICR, as can be seen from table 1. The torque, non-dimensionalized as a pseudo-Nusselt number $Nu_\omega = J^\omega/J^\omega_{pa}$, where J^ω_{pa} is J^ω for the purely azimuthal flow, is approximately a factor four smaller. As a direct consequence of this, the frictional Reynolds number Re_τ is

https://doi.org/10.1017/jfm.2016.400 Published online by Cambridge University Press

1	2	3	4	5	6	7	8	9	10	11
Case	Re_i	Re_o	N_θ	N_r	N_z	Δr^+	Δz^+	$r_i\Delta\theta^+$	$Re_{\tau,i}$	Nu_ω
O0	0	5.5×10^4	384	768	512	0.2–1.6	3.3	6.6	402	11.6 ± 0.2
O1	0	1.1×10^5	384	1024	768	0.2–2.1	3.8	11.5	703	18.3 ± 0.8
O2	0	2.2×10^5	768	1024	1024	0.3–3.6	5.0	9.9	1220	26.2 ± 1.3
I1	1×10^5	0	1024	1024	2048	0.3–4.1	2.7	9.1	1410	69.5 ± 0.2
I2	2×10^5	0	1536	1536	3072	0.3–5.2	3.4	11.4	2660	126 ± 2.1

TABLE 1. Details of the numerical simulations. Column 1 is the name by which the simulation will be referred to in the article. Columns 2 and 3 are the inner and outer cylinder Reynolds numbers. Columns 4–6 represent the numbers of points in the azimuthal, radial and axial directions. Column 7 shows the minimum and maximum resolutions in the radial direction normalized with the inner cylinder wall unit. Columns 8 and 9 show the axial and azimuthal resolutions (at the inner cylinder) in inner cylinder wall units. Column 10 refers to the inner cylinder frictional Reynolds number, and the last column shows the torque non-dimensionalized as a pseudo-Nusselt number.

approximately a factor two lower because $Re_\tau \sim \sqrt{Nu_\omega}$. This results in smaller values of u_τ for pure OCR, and thus the longer transients observed in the DNS.

Transport of angular velocity from across the gap is much more inefficient in the case of subcritical turbulence, something that can be expected from the 'optimal' transport results of van Gils *et al.* (2012) and Paoletti *et al.* (2012), where the driving torque drastically decreases with the appearance of the radial partitioning into subcritical and supercritical zones. However, unlike the quasi-Keplerian case, where $|r_o^2\omega_o| > |r_i^2\omega_i|$ and $|\omega_o| < |\omega_i|$, which were found both numerically (Ostilla-Monico *et al.* 2014*b*) and experimentally (Nordsiek *et al.* 2015) to not sustain angular velocity transport across the gap, in pure OCR there is still turbulence present, and the flow is not purely azimuthal because $Nu_\omega \neq 1$. In the case of pure OCR rotation, the gradients of both angular velocity and angular momentum point in the same direction, i.e. inwards, while in the quasi-Keplerian cases, they point in different directions, i.e. inwards for the angular momentum and outwards for the angular velocity.

To understand why the torque is lower for pure OCR, we visualize the flow field in figure 1, which shows a pseudocolour plot of the instantaneous angular velocity for an azimuthal cut (*a*) and at the mid-gap (*b*) for the O2 case. A complete absence of the large-scale rolls can be seen. These figures can be compared to figures 1 and 3 of Ostilla-Mónico *et al.* (2015), visualizations of the instantaneous velocities for the I1 case. For the same geometrical parameters, and similar Reynolds numbers, the velocities in the pure IRC cases have marked axial inhomogeneities. The existence of rolls has been linked to increased transport (Brauckmann & Eckhardt 2013; Grossmann *et al.* 2016), so from this alone we can expect a smaller Nu_ω.

Figure 2(*a*) shows $\tilde{L}$, the azimuthally, temporally and axially averaged angular momentum for the O0, O1, O2 and I1 cases, as well as the experimental data from Burin & Czarnocki (2012) for $\eta = 0.97$ and $Re_o = 6800$. For pure ICR, rolls effectively redistribute angular momentum such that the flow is marginally stable. This is reflected in the I1 case showing a constant angular momentum profile in the bulk equal to the arithmetic average of L at both cylinders. For pure OCR, the flow is already stable and thus we do not expect rolls to form or angular momentum to be redistributed. Instead, all pure OCR cases show a significant gradient of angular momentum in the bulk. For pure OCR, the larger the angular momentum gradient in

https://doi.org/10.1017/jfm.2016.400 Published online by Cambridge University Press

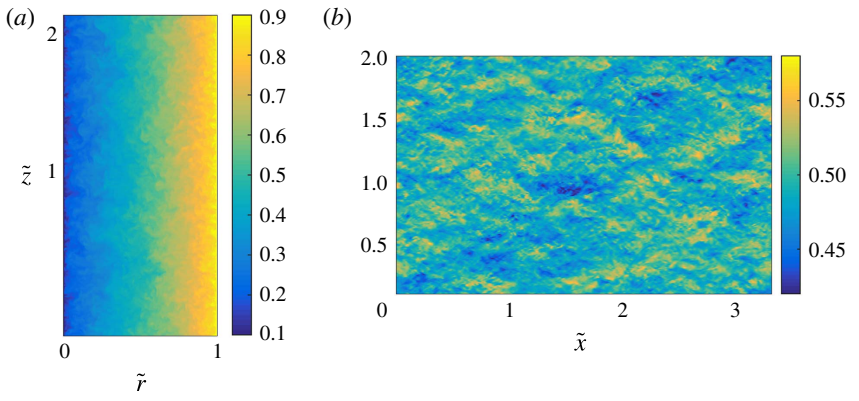

FIGURE 1. Pseudocolour plot of the instantaneous angular velocity for the O2 case for a constant azimuth (*a*) and at the mid-gap (*b*). No large-scale structures can be seen, as is seen for pure inner cylinder rotation in Ostilla-Mónico *et al.* (2015, 2016).

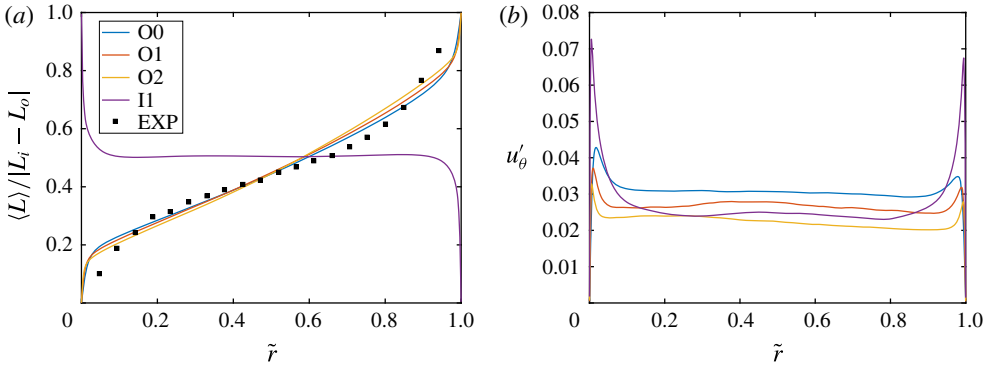

FIGURE 2. (*a*) The temporally, axially and azimuthally averaged angular momentum for the three pure OCR cases and the I1 case for comparison, as well as experimental data from Burin & Czarnocki (2012). (*b*) The root mean square (r.m.s.) of the azimuthal velocity for the numerical cases.

the bulk, the more stable the configuration. The resulting profile shape comes from the competing mechanisms of centrifugal stabilization in the bulk and destabilization in the boundary layers by shear. The numerical pure OCR velocity profiles are in qualitative agreement with the experimental profiles, as the bulk profile becomes flatter and the boundary layers thinner with increasing Re_o. We also note that similar phenomena were seen for the strongly counter-rotating cylinder cases of Brauckmann, Salewski & Eckhardt (2016), which show significant deviations from constant angular momentum profiles in the bulk after the onset of the radial partitioning of stability.

Figure 2(*b*) shows the root mean square (r.m.s.) of the azimuthal velocity u'_θ for the O0, O1, O2 and I1 cases. The level of fluctuations decreases with Reynolds number. When comparing the O1 and the I1 cases, a much lower level of fluctuations inside the boundary layer is seen for pure OCR. This is expected from the much lower values of u_τ for pure OCR than for pure ICR. Indeed, u_τ is approximately a factor of two larger for the I1 case, and this is directly reflected in the level of fluctuations being approximately twice as large as for the O1 case.

https://doi.org/10.1017/jfm.2016.400 Published online by Cambridge University Press

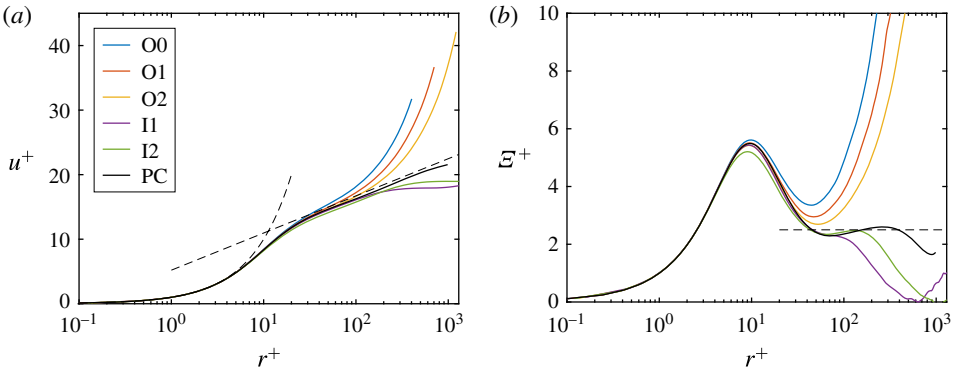

FIGURE 3. (*a*) The streamwise velocity in inner cylinder wall units for all the cases at the inner cylinder, and from PC flow at $Re_\tau \approx 1000$. The dashed curve represents $u^+ = r^+$ and the dashed line represents $u^+ = 2.5\log(r^+) + 5.2$. (*b*) The logarithmic diagnostic function for the cases shown in (*a*). The horizontal dashed line represents $\Xi^+ = 2.5$.

We now focus on the near-wall region, to compare pure OCR with pure ICR, and to quantify the effects of curvature and instability. Figure 3(*a*) shows the mean streamwise velocity at the inner cylinder region in inner units for all cases, where U^+ is $U^+ = (r_i\omega_i - \langle u_\theta\rangle_{\theta,z,t})/u_{\tau,i}$ and r^+ is the distance from the wall in inner cylinder wall units, $r^+ = (r - r_i)/\delta_{\nu,i}$. The simulation of plane Couette (PC) flow at $Re_\tau \approx 1000$ from Pirozzoli, Bernardini & Orlandi (2014) has been added for comparison. Rotating PC flow is the limit of TC flow when $\eta \to 1$, i.e. the two cylinders become two plates. Therefore, curvature effects and centrifugal (de)stabilization are not present. Romanov (1973) showed that PC flow is also stable to linear perturbations at all Reynolds numbers, though the mechanism is not centrifugal and this could cause different behaviour.

Both pure ICR and pure OCR TC flow can be seen to deviate substantially from the classical von Karman law of the wall, $U^+ = \kappa^{-1}\log(y^+) + B$, with $\kappa = 0.4$ and $B = 5.2$, while PC flow follows it better. Pure OCR TC flow has a significantly higher value of U^+ far away from the walls, while pure ICR TC flow has a rather flat profile in the bulk – consistent with the notion that angular momentum is redistributed in the bulk. It seems that while, in the bulk, pure ICR redistributes angular momentum through the rolls, pure OCR has the opposite effect, and generates a strong gradient of angular momentum. Thus, the two lines deviate from the PC profile in opposite ways, showing the importance of the centrifugal (in)stability.

Very close to the wall, it could seem that the O2 case is beginning to show a logarithmic-like region. This can be better seen in figure 3(*b*), which shows the logarithmic diagnostic function $\Xi^+ = \mathrm{d}U^+/\mathrm{d}(\log r^+)$ for the same cases. Even if the pure OCR cases deviate much more than both the PC cases and the pure ICR cases, and do not show the S-like shape in Ξ^+ around $r^+ \approx 100$ that is seen in several canonical flows (Ostilla-Mónico *et al.* 2016), they are coming closer to the classical law of the wall with increasing Re_τ number. It could be that for higher drivings, and thus higher Re_τ, the pure OCR profiles collapse in the near-wall region onto the PC profiles, once the boundary layer is small enough such that it no longer feels the effect of curvature and of the centrifugal stabilization. However, from the figures its seems that the centrifugal (in)stability mechanism plays a critical role in determining the bulk behaviour, and is responsible for the large deviations of TC flow from PC

https://doi.org/10.1017/jfm.2016.400 Published online by Cambridge University Press

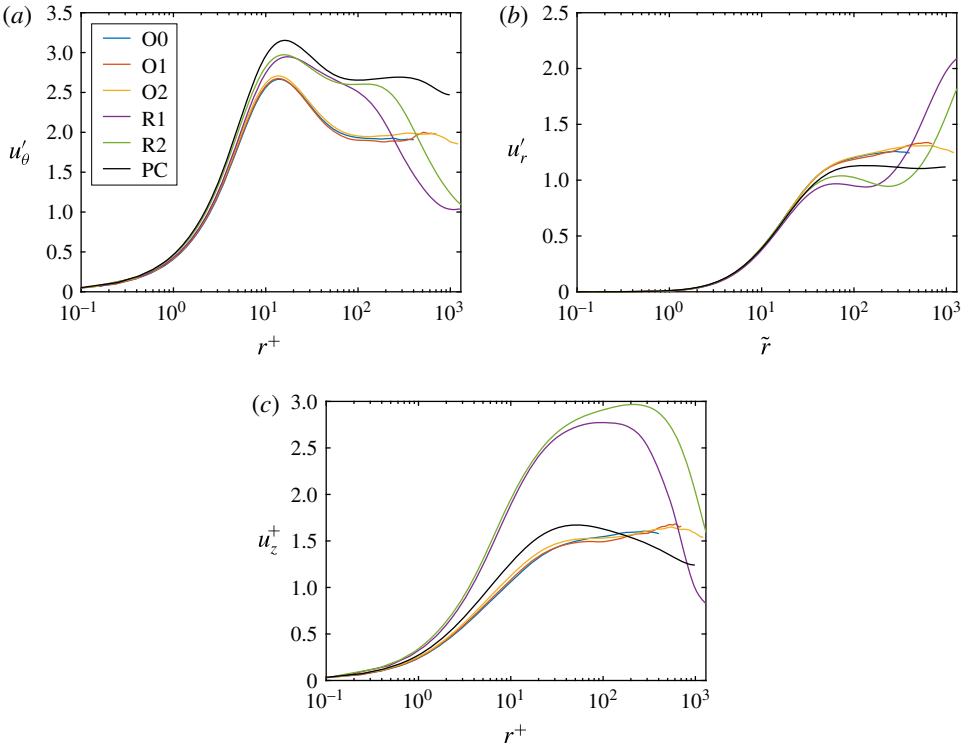

FIGURE 4. Root-mean-squared fluctuations for all cases for the streamwise/azimuthal (*a*), wall-normal/radial (*b*) and spanwise/axial (*c*) velocities in inner cylinder wall units.

flow behaviour. Finally, the outer cylinder wall profiles show very similar behaviour and are not shown here, so the main effects seems to be mediated by the centrifugal (in)stability and not by convex or concave curvature.

We now show the fluctuations in inner cylinder wall units for all three components of velocity in figure 4. While the streamwise fluctuations are considerably smaller for pure OCR, the profiles are closer to those of plane Couette flow for radial (wall-normal) and axial (spanwise) fluctuations. The cases of pure ICR rotation show very strong deviations for these two velocities, attributed to the axial inhomogeneity of the flow in Ostilla-Mónico *et al.* (2016). Again, the outer cylinder wall profiles show very similar behaviour and are not shown here. The significant deviations from PC flow behaviour can be attributed again to the different mechanisms at play, especially centrifugal (de)stabilization.

Finally, to quantify the nature of transport in the boundary layers, figure 5(*a*) shows the pre-multiplied axial spectra of radial and azimuthal velocity for the O2 case at $r^+ \approx 12$, i.e. around the peak of u' fluctuations inside the boundary layer. The peak seen at the roll-wavelength for pure ICR in Ostilla-Mónico *et al.* (2016) is no longer present, as transport occurs through small-scale fluctuations or 'bursts' (Brauckmann & Eckhardt 2013). These bursts transport angular velocity, and are very intermittent, having large amplitude but slow dynamics, meaning that extreme events are more likely to happen. The peak in the radial spectra corresponds to the characteristic length scale of these bursts. We note that spectra seen here are consistent with the spectra seen in channel flow (Jimenez 2012) and in plane Couette flow (Avsarkisov *et al.*

https://doi.org/10.1017/jfm.2016.400 Published online by Cambridge University Press

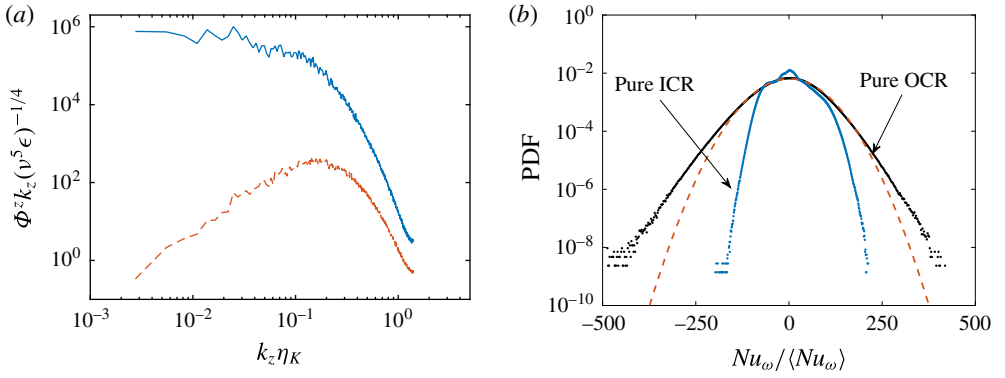

FIGURE 5. (*a*) The axial spectra for the radial (red dashed) and azimuthal (blue solid) velocities for $r^+ \approx 12$, near the inner cylinder, for the O2 case. (*b*) The p.d.f. of Nu_ω at the mid-gap for both the I2 and O2 cases. The orange dashed line represents a Gaussian p.d.f. with mean and variance equal to those of the O2 case.

2014), having a peak in the radial (wall-normal) spectra associated with the size of the transporting structures, and no saturation for the azimuthal velocity, indicating large-scale structures attached to the wall that do not transport Reynolds stresses.

To quantify this feature, figure 5(*b*) shows the probability density function (p.d.f.) of the local convective angular velocity current $u_r\omega \approx Nu_\omega$ for both the O2 and I2 cases at mid-gap, i.e. in the bulk, as well as a Gaussian distribution with mean and variance equal to the O2 case. While for pure ICR, transport occurs mainly through the hairpin vortices, seen as the prominent peak centred around the middle of the graph, for the O2 case, the signature of these bursts is reflected here in the fatter tails of the p.d.f., which are super-Gaussian, and have no apparent power-law behaviour. The p.d.f.s are not symmetric around zero, as there is a net positive angular velocity transport. From both panels, it becomes clear that the mechanisms for angular velocity transport are very different for pure ICR and pure OCR.

4. Summary and conclusions

A series of DNS of turbulent Taylor–Couette flow with pure outer cylinder rotation were conducted. Overall, pure OCR TC flow behaves in a very different manner from supercritical pure ICR TC flow. The torque and fluctuation levels are much smaller for comparable Reynolds numbers than those of pure ICR flow. Transport of angular velocity, now more inefficient, occurs through intermittent ‘bursts’ instead of through the large-scale structures. Pure OCR TC flow can be seen as just an extreme case of counter-rotating TC flow with the radial partitioning of stability described by Brauckmann & Eckhardt (2013) and Brauckmann *et al.* (2016) moving to the inner cylinder. The competition between the shear instabilities in the boundary layer and the centrifugal stabilization in the bulk gives rise to mean velocity profiles that show a significant angular momentum gradient in the bulk, consistent with the experiments of Burin & Czarnocki (2012). The near-wall profiles deviate very strongly from both pure ICR rotation and plane Couette flow, revealing the very strong role of the centrifugal mechanisms in TC flow, be it stabilizing for pure OCR or destabilizing for pure ICR. Pure ICR and pure OCR deviate in opposite manners from the PC flow profiles, so this can be attributed to the role of centrifugal (de)stabilization.

https://doi.org/10.1017/jfm.2016.400 Published online by Cambridge University Press

Finally, the large-scale structures completely disappear in this regime, and the axial velocity spectra reveal that transport near the wall occurs predominantly through very intermittent and small-scale structures.

Two main questions remain: the large-scale rolls seem to form in certain regions of the parameter space, where the flow is fully unstable (Ostilla-Monico *et al.* 2014*a*). However, it is still unclear why these rolls are formed, and why they are axially pinned. From these simulations, it seems that the centrifugal instability plays a clear role in the nature of the turbulence and the formation of the rolls, but a complete understanding is still missing. Furthermore, the question remains of what happens in the quasi-Keplerian regime, which satisfies $|L_o| > |L_i|$ and $|\omega_o| < |\omega_i|$ (Ostilla-Monico *et al.* 2014*b*; Nordsiek *et al.* 2015). The simulations in this article have generated and sustained turbulence in the absence of end plates at high Reynolds numbers. However, turbulence in the quasi-Keplerian regime has not been sustained in simulations, and, as mentioned previously, this could be due to the opposing gradients of angular momentum and angular velocity. We refer the reader to Grossmann *et al.* (2016) for a recent review of the progress on this problem.

Acknowledgements

We thank V. Spandan for extensive help in proof-reading the paper and keeping some simulations running during the months-long wall-clock times, and we thank M. Burin for providing the data for figure 2 and for valuable discussions. We acknowledge Y. Yang and X. Zhu for fruitful and stimulating discussions. We also gratefully acknowledge computational time for the simulations provided by SurfSARA on resource Cartesius through a NWO grant.

References

ANDERECK, C. D., DICKMAN, R. & SWINNEY, H. L. 1983 New flows in a circular Couette system with corotating cylinders. *Phys. Fluids* **26**, 1395–1401.

ANDERECK, C. D., LIU, S. S. & SWINNEY, H. L. 1986 Flow regimes in a circular Couette system with independently rotating cylinders. *J. Fluid Mech.* **164**, 155–183.

VAN ATTA, C. W. 1966 Exploratory measurements in spiral turbulence. *J. Fluid Mech.* **25** (3), 495–512.

AVSARKISOV, V., HOYAS, S., OBERLACK, M. & GARCÍA-GALACHE, J. P. 2014 Turbulent plane Couette flow at moderately high Reynolds number. *J. Fluid Mech.* **751**, R1–8.

BORRERO-ECHEVERRY, D. 2014 Sub-critical transition to turbulence in Taylor–Couette flow. PhD thesis, Georgia Institute of Technology, Atlanta, GA.

BORRERO-ECHEVERRY, D., SCHATZ, M. F. & TAGG, R. 2010 Transient turbulence in Taylor–Couette flow. *Phys. Rev.* E **81**, 025301.

BRAUCKMANN, H., SALEWSKI, M. & ECKHARDT, B. 2016 Momentum transport in Taylor–Couette flow with vanishing curvature. *J. Fluid Mech.* **790**, 419–452.

BRAUCKMANN, H. J. & ECKHARDT, B. 2013 Intermittent boundary layers and torque maxima in Taylor–Couette flow. *Phys. Rev.* E **87** (3), 033004.

BURIN, M. J. & CZARNOCKI, C. J. 2012 Subcritical transition and spiral turbulence in circular Couette flow. *J. Fluid Mech.* **709**, 106–122.

COLES, D. 1965 Transition in circular Couette flow. *J. Fluid Mech.* **21**, 385–425.

DEGUCHI, K., MESEGUER, A. & MELLIBOVSKY, F. 2014 Subcritical equilibria in Taylor–Couette flow. *Phys. Rev. Lett.* **112**, 184502.

DUBRULLE, B., DAUCHOT, O., DAVIAUD, F., LONGARETTI, P. Y., RICHARD, D. & ZAHN, J. P. 2005 Stability and turbulent transport in Taylor–Couette flow from analysis of experimental data. *Phys. Fluids* **17**, 095103.

https://doi.org/10.1017/jfm.2016.400 Published online by Cambridge University Press

ECKHARDT, B., FAISST, H., SCHMIEGEL, A. & SCHNEIDER, T. 2008 Dynamical systems and the transition to turbulence in linearly stable shear flows. *Phil. Trans. R. Soc. Lond.* A **366**, 1297–1315.

ECKHARDT, B., GROSSMANN, S. & LOHSE, D. 2007 Torque scaling in turbulent Taylor–Couette flow between independently rotating cylinders. *J. Fluid Mech.* **581**, 221–250.

FARDIN, M. A., PERGE, C. & TABERLET, N. 2014 The hydrogen atom of fluid dynamics – introduction to the Taylor–Couette flow for soft matter scientists. *Soft Matt.* **10** (20), 3523–3535.

VAN GILS, D. P. M., HUISMAN, S. G., GROSSMANN, S., SUN, C. & LOHSE, D. 2012 Optimal Taylor–Couette turbulence. *J. Fluid Mech.* **706**, 118–149.

GROSSMANN, S., LOHSE, D. & SUN, C. 2016 High-Reynolds number Taylor–Couette turbulence. *Annu. Rev. Fluid Mech.* **48**, 53–80.

HUISMAN, S. G., VAN DER VEEN, R. C. A., SUN, C. & LOHSE, D. 2014 Multiple states in highly turbulent Taylor–Couette flow. *Nat. Commun.* **5**, 3820.

JIMENEZ, J. 2012 Cascades in wall-bounded turbulence. *Annu. Rev. Fluid. Mech.* **44**, 27–45.

NORDSIEK, F., HUISMAN, S. G., VAN DER VEEN, R. C. A., SUN, C., LOHSE, D. & LATHROP, D. P. 2015 Azimuthal velocity profiles in Rayleigh-stable Taylor–Couette flow and implied axial angular momentum transport. *J. Fluid Mech.* **774**, 342–362.

OSTILLA-MONICO, R., VAN DER POEL, E. P., VERZICCO, R., GROSSMANN, S. & LOHSE, D. 2014*a* Exploring the phase diagram of fully turbulent Taylor–Couette flow. *J. Fluid Mech.* **761**, 1–26.

OSTILLA-MONICO, R., VERZICCO, R., GROSSMANN, S. & LOHSE, D. 2014*b* Turbulence decay towards the linearly-stable regime of Taylor–Couette flow. *J. Fluid Mech.* **747**, 1–29.

OSTILLA-MÓNICO, R., VERZICCO, R., GROSSMANN, S. & LOHSE, D. 2016 The near-wall region of highly turbulent Taylor–Couette flow. *J. Fluid Mech.* **768**, 95–117.

OSTILLA-MÓNICO, R., VERZICCO, R. & LOHSE, D. 2015 Effects of the computational domain size on DNS of Taylor–Couette turbulence with stationary outer cylinder. *Phys. Fluids* **27**, 025110.

PAOLETTI, M. S., VAN GILS, D. P. M., DUBRULLE, B., SUN, C., LOHSE, D. & LATHROP, D. P. 2012 Angular momentum transport and turbulence in laboratory models of Keplerian flows. *Astron. Astrophys.* **547**, A64.

PAOLETTI, M. S. & LATHROP, D. P. 2011 Angular momentum transport in turbulent flow between independently rotating cylinders. *Phys. Rev. Lett.* **106**, 024501.

PIROZZOLI, S., BERNARDINI, M. & ORLANDI, P. 2014 Turbulence statistics in Couette flow at high Reynolds number. *J. Fluid Mech.* **758**, 327–343.

VAN DER POEL, E. P., OSTILLA-MONICO, R., DONNERS, J. & VERZICCO, R. 2015 A pencil distributed finite difference code for strongly turbulent wall-bounded flows. *Comput. Fluids* **116**, 10–16.

RAYLEIGH, LORD 1917 On the dynamics of revolving fluids. *Proc. R. Soc. Lond.* A **93**, 148–157.

ROMANOV, V. A. 1973 Stability of plane-parallel Couette flow. *Funct. Anal. Applics.* **7** (2), 137–146.

TAYLOR, G. I. 1923 Experiments on the motion of solid bodies in rotating fluids. *Proc. R. Soc. Lond.* A **104**, 213–218.

TAYLOR, G. I. 1936 Fluid friction between rotating cylinders. *Proc. R. Soc. Lond.* A **157**, 546–564.

VERZICCO, R. & ORLANDI, P. 1996 A finite-difference scheme for three-dimensional incompressible flow in cylindrical coordinates. *J. Comput. Phys.* **123**, 402–413.

https://doi.org/10.1017/jfm.2016.400 Published online by Cambridge University Press